Section 3. Materials Science

https://doi.org/10.29013/EJTNS-22-1.2-17-26

Yiming Huang,
Semiahmoo Secondary School Surrey BC, Canada

ACTIVE BROADBAND PERFECT ABSORBER BASED ON PHASE CHANGE MATERIAL FOR SOLAR ENERGY HARVESTING

Abstract. In this paper, a wide-angle, polarization-independent broadband perfect absorber based on GeTe phase-change materials is reported. It is found that the bandwidth of the absorber reaches 600 nm, and the absorptivity is higher than 90%. Moreover, absorptivity in the range of 400 ~ 1000 nm is higher than 85% when the incident angle is increased from 0 to 40 degrees. Although the geometry size of the absorber is fixed, absorption bandwidth and absorptivity can still be actively adjusted by changing the phase-change degree. The underlying physical mechanism of this absorber is ascribed to the localized surface plasmon resonance of Ag nanopillars as well as the Fabry-Pérot (FP) resonance between GeTe and bottom Ag films. This proposed perfect absorber design has great potential in solar energy harvesting, *etc.*

Keywords: perfect absorber; phase-change material; all-dielectric; tunable; broadband.

1. Introduction

Perfect metamaterial absorber, proposed by Landy *et al.* [1] in 2008, can minimize the reflectance and eliminate the transmission. It has recently attracted many interests because of its potential value in areas such as energy harvesting [2–4], sensors [5], thermal emitters [6], *etc.* So far, perfect absorber can be operated in visible frequencies [7; 8], terahertz regime [6], and near infrared region [9]. At the same time, the perfect absorber can also achieve narrowband and broadband absorption for practical requirements [5, 10]. For example, narrowband absorber can be used as sensors [11] while broadband absorber can be utilized for solar energy harvesting [12].

With the increment challenge of environmental pollution and gradual aggravation of the energy crisis, sustainable clean energy, particularly the solar energy, has attracted more and more attention. However, the high-efficient use of solar energy requires appropriate energy collector, and current energy collectors suffer from bulky volume and inconvenience. Perfect broadband absorber based on metamaterial can effectively address above-mentioned problems and possesses the merits of small and light weight. Currently, many researchers have proposed various broadband absorbers for solar energy harvesting. L. Zhu, *et al.* designed a broadband absorber made of a ring column and dual hexagon pillar for solar energy harvesting [13]. The designed absorber obtained the absorptivity of 96% in 300 ~ 1300 nm wavelengths range and the absorptivity of 95% in the whole visible to near-infrared wavelength. C. Ma, *et al.* demonstrated a broadband absorber containing tellurium nanoparticles that can absorb more than 85% solar energy in the wavelength of 200 ~ 2000 nm and can achieve efficient photothermal conversion [14]. M. Bagmanci, *et al.* designed a broadband absorber composed of a nickel-SiO_2–nickel array with the absorptivity of more than 91% at the

whole visible light spectrum and even the absorptivity of 99% between 556 and 657 THz [15]. However, all these reported absorbers have a single function and cannot realize tunability once structure design is fixed.

Fortunately, chalcogenide phase change material (*e.g.,* Ge Te) is a promising active media that can be employed in the absorber design. This is owing to that phase change material possesses large contrasts in refractive index and extinction coefficient between amorphous and crystalline states at optical, electric or thermal stimulus [16–18]. Therefore, the broadband absorber based on phase change material may provide tunability of absorbance performance in despite of the fixed structure design. Here, an active broadband absorber based on Ge Te phase change material is proposed for solar energy harvesting. Since the electromagnetic wave energy of solar radiation is mainly concentrated in the visible-near infrared band, the optical absorption characteristics ranged from 400 to 1000 nm in our designed absorber are theoretically investigated in detail. The influence of structural parameters and phase change process on the absorption performance is obvious. Lastly, the physical mechanism of perfect absorber is analyzed.

2. Structural design and computation

The designed perfect absorber is made of bottom Ag thin film, middle GeTe thin film, and top Ag nanopillar as shown in (Fig. 1). The bottom Ag and middle GeTe thin films have the thicknesses of d_{GeTe} and d_{Ag}, respectively. The top Ag nanopillar has the period, radius, and height of p, r_{Ag} and h_{Ag}, respectively, as displayed in the side view of Fig.1a and the top view of (Fig. 1 b). The bottom Ag thin film is mainly used as a reflective layer to prevent the light transmitted.

In this work, GeTe phase change material is used as an active layer because of its substantial difference of refractive index and extinction coefficient after the phase transition from amorphous to crystalline state [19; 20]. Ag nanopillar is acted as functional structure owing to its surface plasma effect. (Fig. 20) shows the optical properties of Ag and GeTe thin films, which can be extracted by related references [9, 20]. In (Fig. 2 a and b), the dielectric constants of Ge Te films with various crystallization degree can be obtained by optical, electric or thermal stimulus.

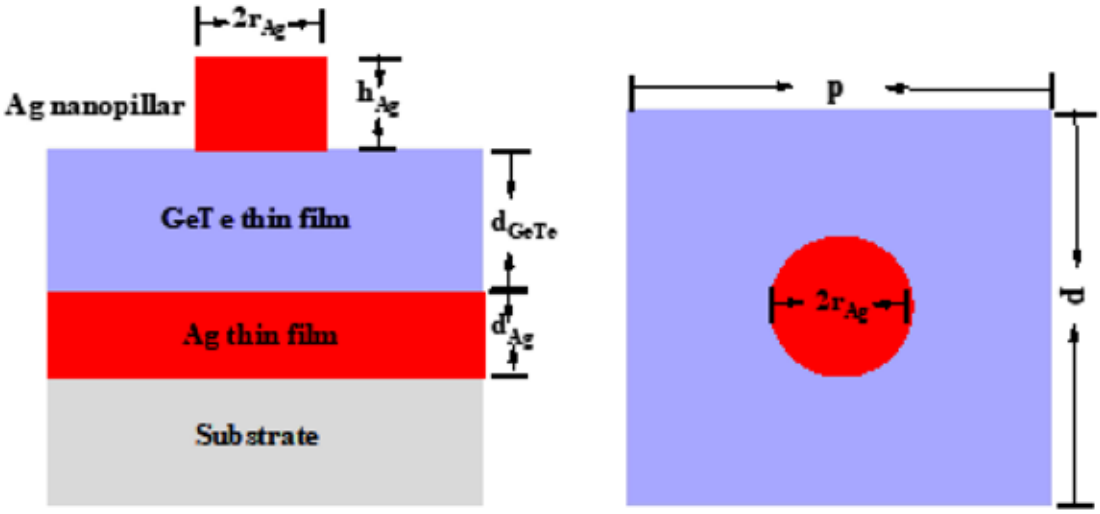

a) b)

Figure 1. The designed structure of broadband perfect absorber. (a) – side view; (b) – top view

The proposed broadband absorber can be computed via setting the structural and material parameters by a commercial COMSOL software. The absorption performance of absorber is evaluated

according to the simulated absorbance spectra at the 400~1000 nm wavelength. In the theoretical simulation, the incident light is set under p-polarized (TM, the electric field is incident in x axis) and s-polarized (TE, the electric field is incident in y axis) direction.

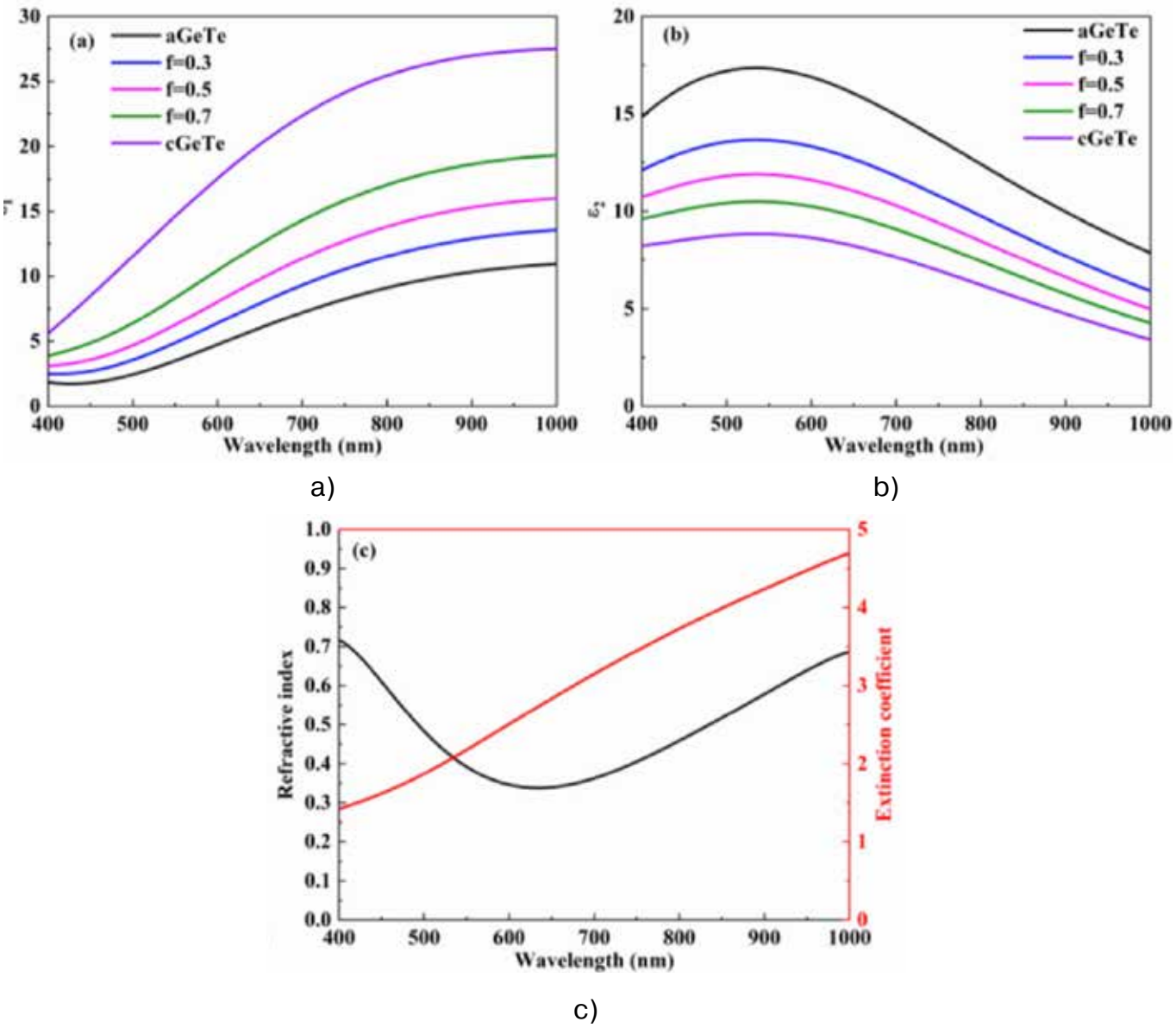

a) b) c)

Figure 2. The dielectric constants (ε_1 and ε_2) of amorphous and crystalline GeTe thin films (labeled as aGeTe and cGeTe), where *f* stands for crystallization fraction, obtained from Ref [20]. (c) Optical constants (refractive index and entinction coefficient) of Ag thin film [9]

The excitation port is set in *z* direction, and the periodic boundary conditions are set in x and y directions to simulate the infinite nanopillars, and perfect matching layers are set in z direction.

3. Results and Discussions

Fig. 3 a examines the absorption spectra of the perfect absorbers when the Ag nanopillars are set at various heights. In this scenario, the period and radius of the Ag nanopillars are 350 nm and 50 nm. The thickness of the Ge Te layer is 40 nm, and for the bottom Ag layer it is 200 nm.

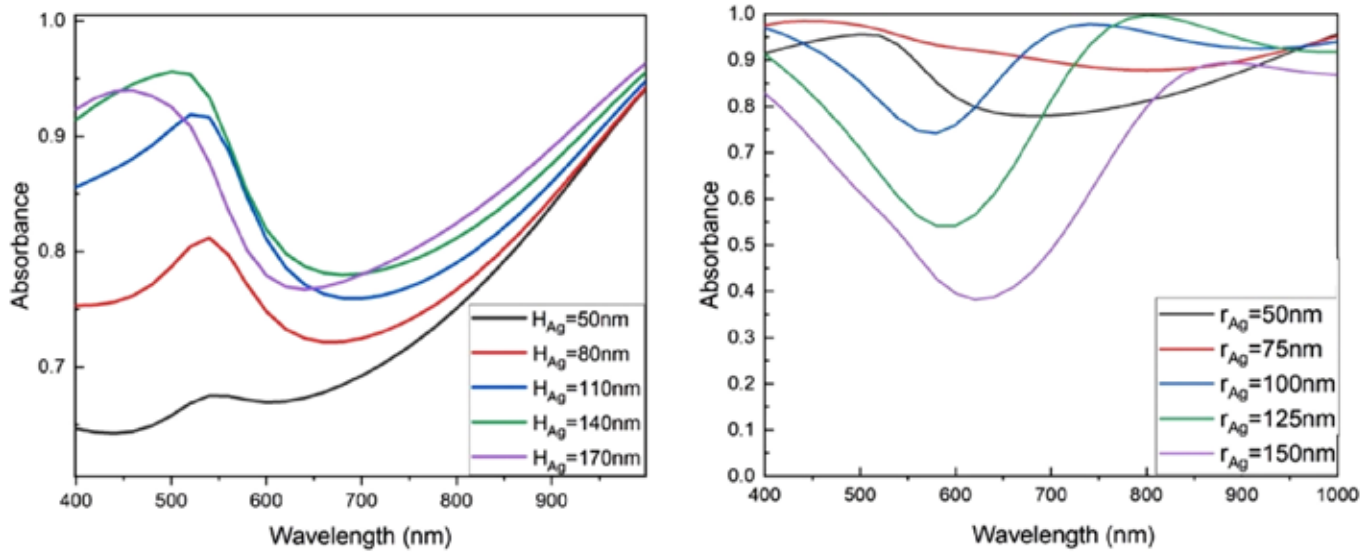

a) b)

Figure 3. Absorption spectra of the designed perfect absorbers using (a) – different heights h_{Ag} and (b) – different radiuses r_{Ag} of Ag nanopillars. In (a), p=350 nm, r_{Ag}= 50 nm, d_{aGeTe}=40 nvm, d_{Ag}=200 nm. In (b) p=350 nm, h_{Ag}=140 nm, d_{aGeTe}=40 nm, d_{Ag}=200 nm

It is shown that the absorptivity increases greatly when wavelength is between 400~600 nm while the height of the Ag nanopillars is increased from 50~ ~140 nm, but then decreases slightly when the height raises to 170 nm. During this interval, absorptivity from all the heights peaked between 500~600 nm. On the other hand, the absorptivity between 600~1000 nm slowly increases in a steady curve. Fig. 3 b shows the absorption spectra of the absorbers with different radiuses of Ag nanopillars. Here, the period and the height of the Ag nanopillars are 350 nm and 140 nm, respectively, and the thicknesses of the middle aGeTe and bottom Ag layers are 40 nvm and 200 nvm, respectively. The absorptivity increases at first but then decreases as the radius of the nanopillars increases. When the radius is equal to 75 nm, the absorptivity in the range of 400 ~ 1000nm is always higher than 85%.

To increase the absorptivity of the device even further, the thicknesses of the middle aGeTe and the bottom Ag films, along with the period of the Ag nanopillars, are optimized as shown in (Fig. 4. Fig. 4 a) shows the influence of changes in the thickness of middle aGeTe on the absorptivity of the device. The period, radius and height of the Ag nanopillar are set to be 350 nm, 75 nm and 140 nm, respectively. Finally, the thickness of the bottom Ag layer is set as 200 nm. As shown in the figure, when increasing the aGeTe thickness, the absorptivity in the wavelength range of 400 ~ 600 nm hardly shifts, while the absorptivity in the wavelength range of 600 ~ 1000 nm increases but then reduces shortly after. In addition, when the thickness of aGeTe film is 30 nm, the absorptivity in the range of 400 ~ 1000 nm is consistently higher than 85%. Fig.4b demonstrates the influence of period on the absorptivity of the device. It is shown that the absorptivity in the wavelength range of 400 ~ ~ 700 nm increases dramatically while the absorptivity in 700 ~ 1000 nm wavelength decreases slightly as the period increases. When the period is 350 nm, the absorptivity between wavelength range 400 ~ ~ 1000 nm is above 85%. Lastly, (Fig. 4 c) investigates the influences of the thickness of bottom Ag thin film on the absorptivity of the device. When the thickness of the Ag film is higher than 100 nm, as shown, the absorption in the wavelength range of 400 ~ 1000 nm hardly changes, whereas the absorptivity decreases

when the Ag thickness is lower than 100 nm. It can be explained that a part of the light is transmitted through the device when the Ag film is too thin, resulting in a decrease in absorptivity. Therefore, in order to improve the absorptivity of the device, the thickness of the Ag thin film should be higher than 100 nm. ***

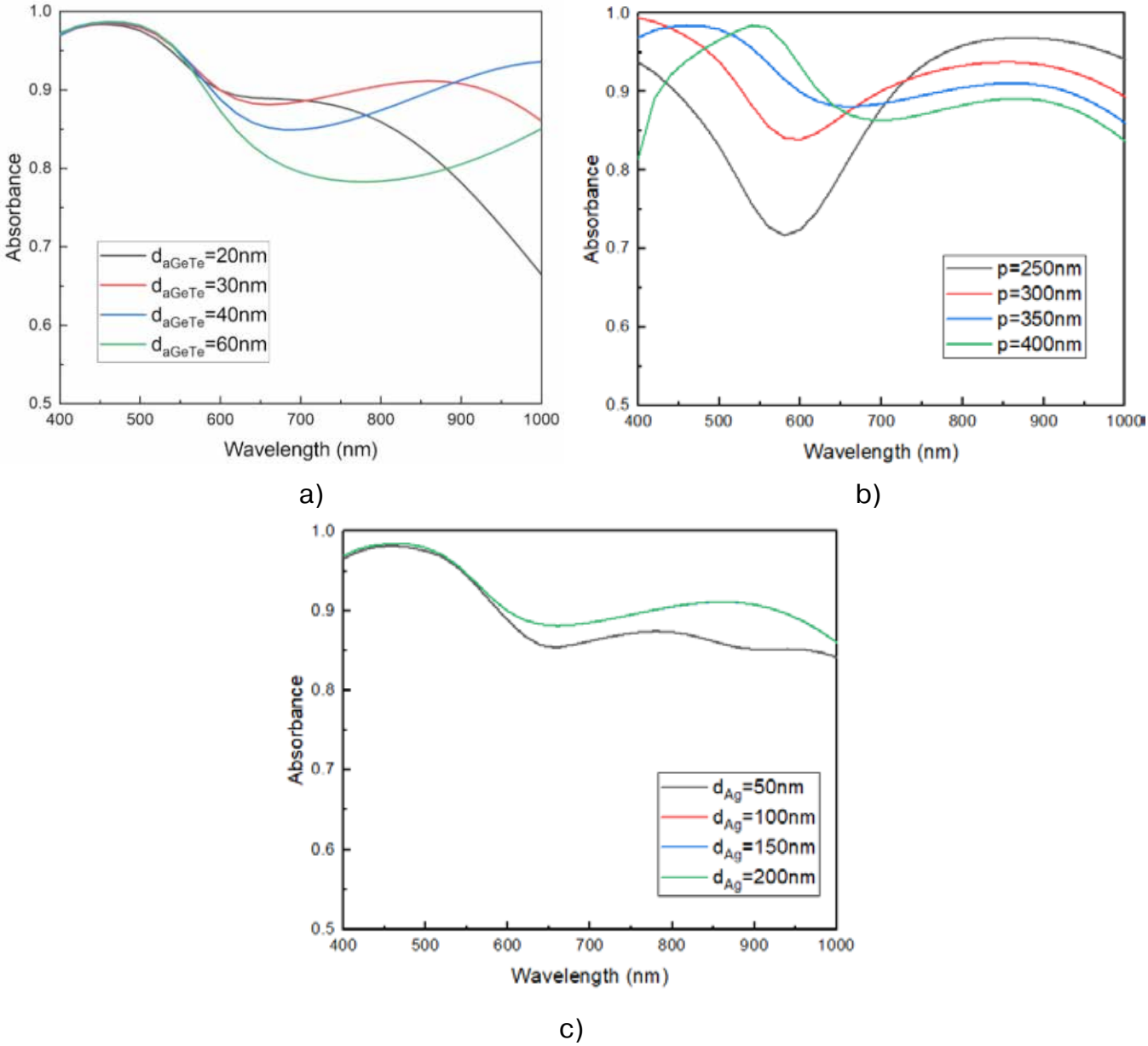

Figure 4. Absorption spectra of the design perfect absorber with (a) – different aGeTe thicknesses, (b) – period p, and (c) – Ag thicknesses d_{Ag}. For (a), p=350 nm, r_{Ag}=75 nm, h_{Ag}=140 nm, d_{Ag}=200 nm. For (b), r_{Ag}=75 nm, h_{Ag}=140 nm, d_{aGeTe}=30 nm, d_{Ag}=200 nm. For (c), p=350 nm, r_{Ag}=75 nm, h_{Ag}=140 nm, d_{aGeTe}=30 nm

Fig. 5 a gives the absorption spectra of the perfect absorbers at different polarizations. Inset is the schematic diagram of the polarization direction. In the device, the period, radius and height of the Ag nanopillar are 350 nm, 75 nm and 140 nm, respectively. Two obvious absorption peaks at 460 nm and 860 nm, and the absorptivity is over 85% in the wavelength range of 400 ~ 1000 nm. Moreover, the absorption curves are the same at both *x* and *y* polarization direction, indicating the polarization-

independent performance of the perfect absorber. Meanwhile, the designed absorber possesses high absorptivity, more than 85%, in the range of 400 ~ 1000 nm. In order to investigate the influence of each layer in the absorption spectra, Fig. 5 b shows the absorption spectra of single Ag thin film, aGeTe/Ag double-layer, Ag nanopillar/Ag film double-layer, and AG nanopillar/aGeTe/Ag thin film three-layer, respectively. It is evident that a single Ag film results in very poor absorptivity. When the aGeTe layer is added onto the Ag film, absorptivity is increased (>80%) at ~ 900 nm wavelength, while the absorptivity at ~ 450 nm can be increased to almost 100% when the Ag nanopillar is added onto the Ag film. When combining the Ag nanopillar, Ag thin film and aGeTe layer, the absorptivity in the wavelength range of 400 ~ 1000 nm can reach above 85%, as shown in the graph.

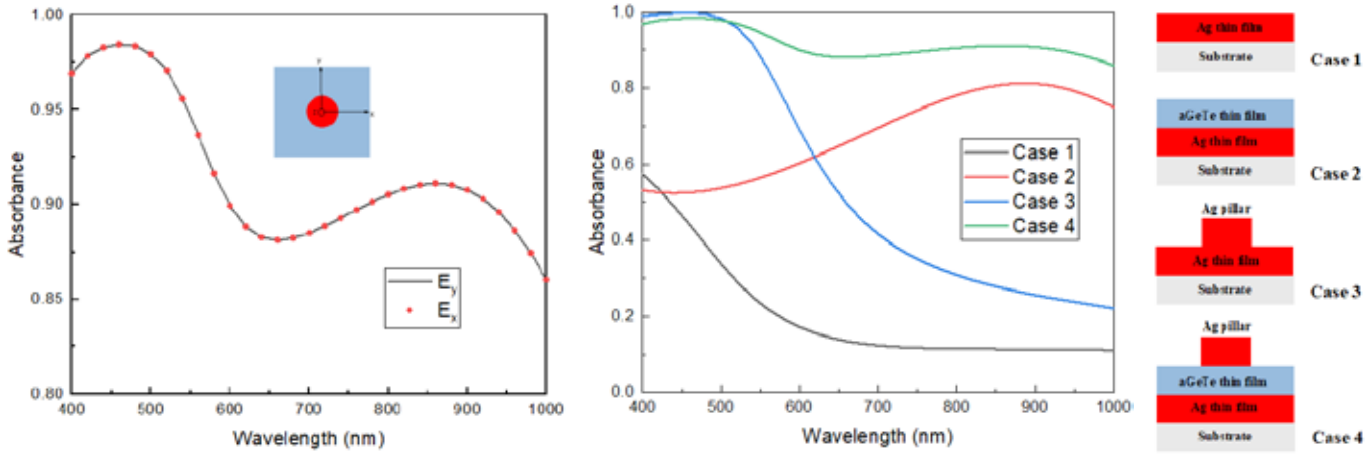

a) b)

Figure 5. Absorption spectra of the designed absorber with (a) – different polarization direction and (b) – each structure. For both (a) and (b), p=350nm, r_{Ag}=75 nm, h_{Ag}= 140 nm, d_{aGeTe}=30 nm, d_{Ag}=150 nm

In order to understand the underlying physics of the broadband perfect absorption, Fig.6 shows the electromagnetic field distributions of the absorbers at wavelengths 460 nm and 860 nm, respectively. The choice of these two wavelengths is due to the absorption peaking at these values, shown in Fig. 5 a. From (Fig. 6 a and 6 b), it is found that at the wavelength of 460 nm, the electric and magnetic fields are concentrated mainly around the edge and the top of the Ag nanopillar in the air layer. This suggests that the absorption peak at 460 nm is ascribed to the localized surface plasma resonance of Ag nanopillars [21]. On the other hand, at the wavelength of 860 nm, as shown in (Figs. 6 c and 6 d), magnetic field is the strongest between Ag nanopillar and aGeTe films along with aGeTe and bottom Ag films, which is consistent with the features of Fabry-Pérot (FP) resonance [21]. The electric field at 860 nm is also concentrated onto the top edge of the Ag nanopillar, causing electric resonance around the Ag nanopillar. Therefore, tailoring the modes of electric and magnetic resonances can achieve broadband absorption.

Incident angle is also an important factor that can affect the absorptivity of the device. The effect of incident angle on the absorptivity of the designed absorber is estimated as shown in (Fig. 7 a). It is obvious that the absorptivity across all incident angles from 0° to 40° is always higher than 80%. This indicates that the designed perfect absorber maintains excellent absorption performance in a wide-angle range. In general, once the geometric size of the absorber is fixed, its function is hardly changed. In this work, however, the

absorption performance can be tuned actively by changing the phase-change degree of the GeTe film at optical, electric or thermal stimulus, even though the device structure is fixed.

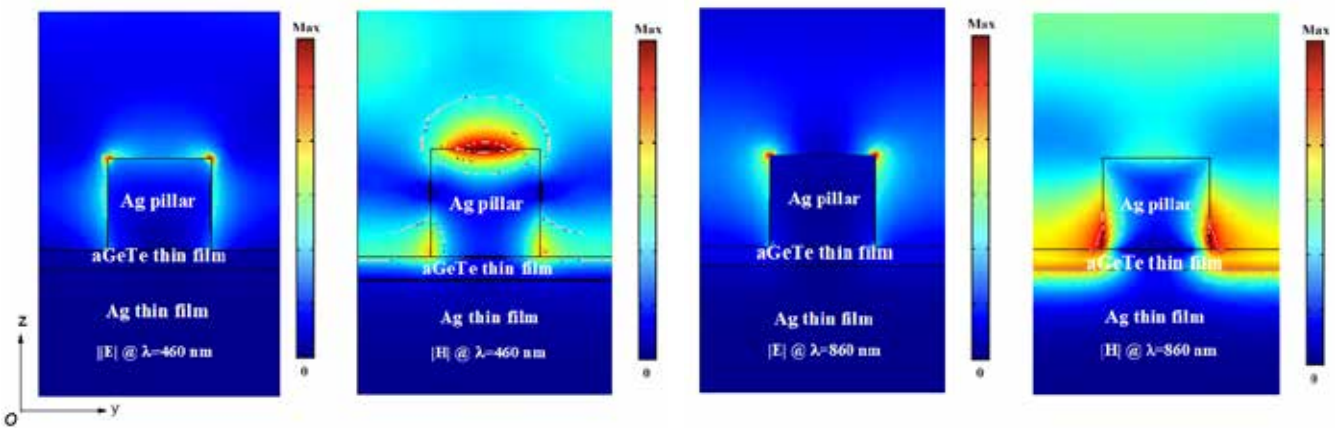

Figure 6. Electromagnetic field distributions of the designed absorbers at the wavelength of 460 nm and 860 nm

In (Fig. 7 b), the absorption spectra of the device with different crystallization degrees are shown. It can be found that the phase-change process obviously influences the absorptivity between 600 ~ 1000 nm while the absorption between 400 ~ 600 nm hardly changed. The absorptivity increases at first but then decreases while the crystallization fraction is increased from 0 to 1. The maximum absorptivity, that is, higher than 90%, is achieved when the crystallization fraction equals to 0.5. In other words, broadband absorption of the device can be adjusted actively via optical, electric or thermal stimulus.

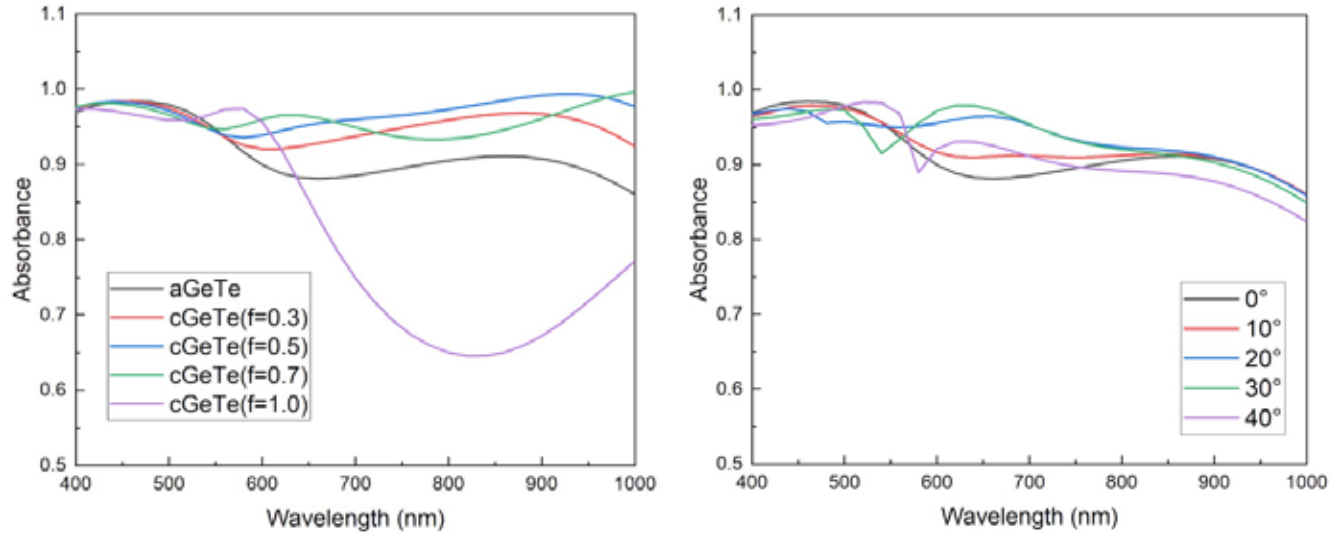

Figure 7. The (a) influence of incident angle and (b) phase change on absorption spectra. For both (a) and (b), p=350nm, r_{Ag}=75 nm, h_{Ag}=140 nm, d_{aGeTe}=20 nm, d_{Ag}=150 nm

In order to investigate the physical mechanism of the absorber after full phase change (f=1.0), the electromagnetic fields of the absorber at the wavelength of 400 nm and 580 nm, respectively. Here, the choice of these two wavelengths is due to the maximum absorption peaks shown in the green line of (Fig. 7 b). From (Fig. 8 a and 8 b) that at the wavelength of 400 nm, both the electric and magnetic fields are concentrated mainly around the Ag nanopillar in the air layer because of the localized surface plasma reso-

nance of the Ag nanopillars. In addition, the electric and magnetic field at 580 nm is also concentrated around the Ag nanopillar and presents the feature of the localized surface plasma resonance as shown in (Fig. 8 c and 8 d) [21]. Moreover, the feature of the Fabry-Pérot (FP) resonance between cGeTe and bottom ag films disappeared. This results in the narrower absorption bandwidth. Therefore, the bandwidth of the perfect absorber can be freely adjusted by the phase change of GeTe films.

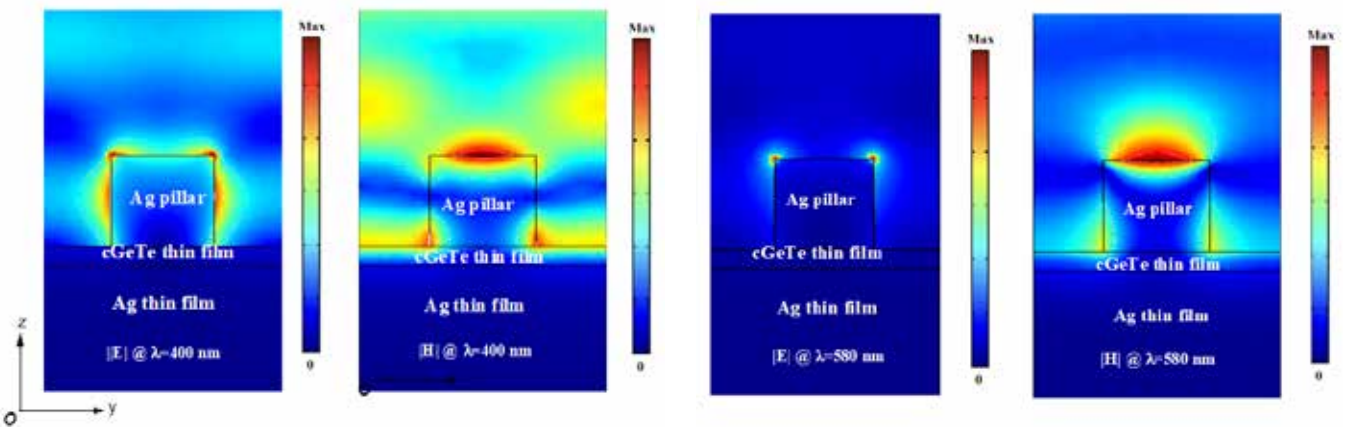

Figure 8. Electromagnetic field distributions of the absorbers at the wavelength of 400 nm and 580 nm

4. Conclusions

In summary, a polarization-independent, wide-angle broadband perfect absorber based upon GeTe phase-change material has been achieved. The structure of the absorber is optimized by changing its geometry parameter (height, radius and period of Ag nanopillar, thickness of GeTe and bottom Ag films). The bandwidth can reach up to 600 nm with an absorptivity higher than 90%. The absorptivity in the range of 400 ~ 1000 nm is consistently higher than 85% when the incident angles increase from 0 ° to 40 °. In particular, absorption bandwidth and absorptivity can be adjusted by tuning the phase-change degree, even though the overall geometry shapes of the absorber is fixed. The underlying mechanism of the absorber is also analyzed in detail. He broadband absorption owes to the combination of both the localized surface plasma resonance of Ag nanopillars and the Farby-Pérot (FP) resonance between GeTe and bottom ag films. Overall, the proposed perfect absorber has great potential in harvesting solar energy through its high absorptivity.

References

1. Qin F., Chen X., Yi Z., Yao W., Yang H., Tang Y., Yi Y., Li H., Yi Y. Ultra-broadband and wide-angle perfect solar absorber based on TiN nanodisk and Ti thin film structure. Solar Energy Materials and Solar Cells,– 211. 2020.– 110535 p.
2. Xiao S., Wang T., Liu T., Zhou C., Jiang X., Zhang J. Active metamaterials and metadevices: a review. Journal of Physics D: Applied Physics,– 53 (50). 2020.– 503002 p.
3. Jahani S., Jacob Z. All-dielectric metamaterials. Nature nanotechnology.– 11 (1). 2016.– P. 23–36.
4. Padilla W. J., Basov D. N., Smith D. R. Negative refractive index metamaterials. Materials Today,– 9(7–8). 2006.– P. 28–35.
5. Wang Q., Yuan G. H., Kiang K. S., Sun K., Gholipour B., Rogers E. T. F., Huang K., Ang S. S., Zheludev N. I., Teng J. H. Reconfigurable phase-change photomask for grayscale photolithography. Applied Physics Letters.– 110 (20). 2017.– 201110 p.

6. Karvounis A., Gholipour B., MacDonald K. F., Zheludev N. I. All-dielectric phase-change reconfigurable metasurface. Applied Physics Letters.– 109(5). 2016.– 051103 p.
7. Landy N. I., Sajuyigbe S., Mock J. J., Smith D. R., Padilla W. J. Perfect metamaterial absorber. Phys Rev Lett.– 100(20). 2008.– 207402 p.
8. Pan M., Su Z., Yu Z., Wu P., Jile H., Yi Z., Chen Z. A narrowband perfect absorber with high Q-factor and its application in sensing in the visible region. Results Phys. 2020.– 19 p.
9. Liang C., Yi Z., Chen X., Tang Y., Yi Y., Zhou Z., Wu X., Huang Z., Yi Y., Zhang G. Dual-Band Infrared Perfect Absorber Based on a Ag-Dielectric-Ag Multilayer Films with Nanoring Grooves Arrays. Plasmonics.– 15 (1), 2019.– P. 93–100.
10. Yi Z., Liu L., Wang L., Cen C., Chen X., Zhou Z., Ye X., Yi Y., Tang Y., Yi Y., Wu P. Tunable dual-band perfect absorber consisting of periodic cross-cross monolayer graphene arrays. Results Phys.– 13, 2019.– 102217.
11. Gao H., Peng W., Liang Y., Chu S., Yu L., Liu Z., Zhang Y. Plasmonic Broadband Perfect Absorber for Visible Light Solar Cells Application. Plasmonics. – 15(2), 2019. – P. 573–580.
12. Deng H., Li Z., Stan L., Rosenmann D., Czaplewski D., Gao J., Yang X. Broadband perfect absorber based on one ultrathin layer of refractory metal. Optics letters, – 40(11). 2015. – P. 2592–5.
13. Mou N., Liu X., Wei T., Dong H., He Q., Zhou L., Zhang Y., Zhang L., Sun S. Large-scale, low-cost, broadband and tunable perfect optical absorber based on phase-change material. Nanoscale, – 12. 2020. – P. 5374–5379.
14. Huang Y., Pu M., Gao P., Zhao Z., Li X., Ma X., Luo X. Ultra-broadband large-scale infrared perfect absorber with optical transparency. Applied Physics Express, – 10 (11). 2017. – 112601 p.
15. Liu Z., Zhong H., Zhang H., Huang Z., Liu G., Liu X., Fu G., Tang C. Silicon multi-resonant metasurface for full-spectrum perfect solar energy absorption. Sol. Energy, – 199. 2020. – P. 360–365.
16. Charola S., Patel S. K., Parmar J., Ladumor M., Dhasarathan V. Broadband graphene-based metasurface solar absorber. Microw Opt Technol Lett. – 62(3). 2020. – P. 1366–1373.
17. Lei L., Li S., Huang H., Tao K., Xu P. Ultra-broadband absorber from visible to near-infrared using plasmonic metamaterial. Optics express, – 26(5). 2018. – P. 5686–5693.
18. Jalil S. A., Lai B., ElKabbash M., Zhang J., Garcell E. M., Singh S., Guo C. Spectral absorption control of femtosecond laser-treated metals and application in solar-thermal devices. Light Sci Appl. – 9. 2020. – 14 p.
19. Luo M., Shen S., Zhou L., Wu S., Zhou Y., Chen L. Broadband, wide-angle, and polarization-independent metamaterial absorber for the visible regime. Optics express, – 25(14). 2017. – P. 16715–16724.
20. Qi B., Zhao Y., Niu T., Mei Z. Ultra-broadband metamaterial absorber based on all-metal nanostructures. Journal of Physics D: Applied Physics, – 52(42). 2019. – 425304 p.
21. Cui Y., Fung K. H., Xu J., Ma H., Jin Y., He S., Fang N. X. Ultrabroadband Light Absorption by a Sawtooth Anisotropic Metamaterial Slab. Nano Lett. – 12(3). 2012. – P. 1443–1447.
22. Yin X., Chen L., Li X. Ultra-Broadband Super Light Absorber Based on Multi-Sized Tapered Hyperbolic Metamaterial Waveguide Arrays. J. Lightwave Technol. – 33(17). 2015. – P. 3704–3710.
23. Wuttig M. Phase change materials: Chalcogenides with remarkable properties due to an unconventional bonding mechanism. physica status solidi (b) – 249(10). 2012. – P. 1843–1850.
24. Ielmini D., Lacaita A. L. Phase change materials in non-volatile storage. Materials Today, – 14(12). 2011. – P. 600–607.
25. Burr G. W., Breitwisch M. J., Franceschini M., Garetto D., Gopalakrishnan K., Jackson B., Kurdi B., Lam C., Lastras L. A., Padilla A., Rajendran B., Raoux S., Shenoy R. S. Phase change memory technology. J. Vac. Sci. Technol. – 28(2). B2010. – P. 223–262.

26. Dong W., Qiu Y., Zhou X., Banas A., Banas K., Breese M. B. H., Cao T., Simpson R. E. Tunable Mid-Infrared Phase-Change Metasurface. Advanced Optical Materials, – 6(14). 2018. – P. 1701346.
27. Du K., Cai L., Luo H., Lu Y., Tian J., Qu Y., Ghosh P., Lyu Y., Cheng Z., Qiu M., Li Q. Wavelength-tunable mid-infrared thermal emitters with a non-volatile phase changing material. Nanoscale, – 10(9). 2018. – P. 4415–4420.
28. Wang J., Li Q., Tao S., Xia Z., Li Y., Liu Y., Gu Z., Hu C. Improving the reflectance and color contrasts of phase-change materials by vacancy reduction for optical-storage and display applications. Opt. Lett. – 45(1). 2020. – P. 244–247.
29. Jafari M., Guo L. J., Rais-Zadeh M. A Reconfigurable Color Reflector by Selective Phase Change of GeTe in a Multilayer Structure. Advanced Optical Materials, – 7(5). 2019. – P. 1801214.